IEEE Access
Multidisciplinary | Rapid Review | Open Access Journal

Received May 20, 2018, accepted June 22, 2018, date of publication June 26, 2018, date of current version July 12, 2018.

Digital Object Identifier 10.1109/ACCESS.2018.2850816

Suppression Approach to Main-Beam Deceptive Jamming in FDA-MIMO Radar Using Nonhomogeneous Sample Detection

LAN LAN[1], GUISHENG LIAO[1], (Senior Member, IEEE), JINGWEI XU[1], (Member, IEEE), YUHONG ZHANG[2], (Senior Member, IEEE), AND FRANCESCO FIORANELLI[3], (Member, IEEE)

[1]National Laboratory of Radar Signal Processing, Xidian University, Xi'an 710071, China
[2]School of Electronic Engineering, Xidian University, Xi'an 710071, China
[3]School of Engineering, University of Glasgow, Glasgow G128QQ, U.K.

Corresponding author: Lan Lan (lanlan_xidian@foxmail.com)

This work was supported in part by the National Key Research and Development Program of China under Grant 2016YFE0200400, in part by the National Nature Science Foundation of China under Grant 61621005, and in part by the China Postdoctoral Science Foundation under Grant 2016M590925 and Grant 2017T100728.

ABSTRACT Suppressing the main-beam deceptive jamming in traditional radar systems is challenging. Furthermore, the observations corrupted by false targets generated by smart deceptive jammers, which are not independent and identically distributed because of the pseudo-random time delay. This in turn complicates the task of jamming suppression. In this paper, a new main-beam deceptive jamming suppression approach is proposed, using nonhomogeneous sample detection in the frequency diverse array-multiple-input and multiple-output radar with non-perfectly orthogonal waveforms. First, according to the time delay or range difference, the true and false targets are discriminated in the joint transmit–receive spatial frequency domain. Subsequently, due to the range mismatch, the false targets are suppressed through a transmit–receive 2-D matched filter. In particular, in order to obtain the jamming-plus-noise covariance matrix with high accuracy, a nonhomogeneous sample detection method is developed. Simulation results are provided to demonstrate the detection performance of the proposed approach.

INDEX TERMS Main-beam deceptive jamming, false targets, frequency diverse array radar, joint range-receive spatial frequency domain, nonhomogeneous sample detection, non-perfectly orthogonal waveforms, transmit-receive 2-D matched filter.

I. INTRODUCTION

In modern electronic warfare, electronic countermeasures (ECMs) have undergone rapid developments, which results in many challenges and threats to the usage of radar systems [1]–[3]. Among ECMs techniques, the deceptive jamming plays a significant role. Particularly, if the deceptive jamming is located within the main-beam, it can cause a severe distortion of the beam-pattern and reduces the estimation precision and tracking accuracy of the victim radar system. Specifically, false targets are a common form of deceptive jamming. Usually, the radar waveform is replicated and delayed by the false target generator (FTG) to confuse the radar system, making it difficult to distinguish true and false targets. The waveform interception can be implemented by using a digital radio frequency memory (DRFM) repeat jammer via properly scaling, delaying, modulating, and retransmitting the intercepted radar waveform [4]–[6]. The maturity of DRFM technology significantly enhances deception capabilities, because the false target echo is robustly correlated with the true target echo. Moreover, based on appropriate DRFM timing, it is possible to produce false target echoes with both negative and positive range offsets [6]. Thus, it is a big challenge to classify and suppress the intended false targets and there is a need for techniques to counteract this problem.

A. RELATED WORKS

In order to restore the performance of radar systems affected by ECMs, electronic counter-countermeasures (ECCMs) capability have been developed [7]. There are generally two

strategies: preventing the radar receiver to receive the jamming signals, and extracting the target from the jamming using the characteristics of the echoes when the received data is corrupted.

Various agility techniques have been proposed to suppress main-beam deceptive jamming, exploiting the fact that this usually lags being the transmitted pulse by at least one pulse repetition interval (PRI), as the jammer needs to use at least one pulse of the intercepted waveform. These techniques search for information difference between true and false targets in different domains, such as pulse agility [8], [9], polarization agility [10], orthogonal waveforms [11], frequency agility [12] and velocity properties [13]. Furthermore, a spatial-correlation processing technique was proposed in [14] for concentrative radar network. In [15], distinction between true targets from false ones was achieved based on the difference of the scattering properties. However, techniques based on the pulse agility in [8] and [9] may result in a high range side lobe and degrade the signal-to-jamming ratio. The approach based on the polarization agility in [10] becomes invalid when the jammer uses polarization modulation and requires practical further considerations on the fluctuation of the signal. Furthermore, due to modulation of the jamming and limited degrees-of-freedom (DOFs) available in traditional radar systems, these methods may not be easily applied in practical scenarios. Hence, there is an urgent need to develop techniques exploiting emerging radar frameworks to achieve extra DOFs.

In this paper, we propose a method for main-beam deceptive jamming suppression from the perspective of waveform design in emerging radar frameworks, in particular using the multiple-input multiple-output (MIMO) radar with frequency diverse array (FDA). Recently, the frequency diverse array (FDA) radar approach has been investigated from different perspectives, including the properties of the transmitted beam-pattern [16]–[19], the frequency offset optimization strategies [20]–[24], FDA system design and waveform optimization [25]–[27], FDA-based new radar schemes [28]–[30], applications in practice [31]–[34]. Thanks to the small frequency increment across the array elements, it has been demonstrated to generate a range-angle-dependent beam-pattern, providing additional degrees-of-freedom (DOFs) for range-angle control. Notice that the extra controllable DOFs offered at the transmitter of FDA radar enable to distinguish the true targets from the false ones in the range domain. By combining this with MIMO technique, the transmit waveforms can be separated at the receiver. Thus, the range-angle-dependent transmit steering vector is obtained. Several approaches have been suggested to suppress the deceptive jamming in FDA-MIMO radar schemes. In [35], a subarray-based FDA method was proposed to counteract the deceptive signals. The FDA-MIMO radar configuration with the generalized likelihood ratio test detector was considered to guarantee high rejection probability of deceptive jamming in [36]. In [34], the FDA-MIMO radar was investigated to suppress the deceptive jamming in the joint transmit-receive domain. However, it was assumed that all the false targets generated by an identical FTG had the same steering vector, which cannot be considered as a general case. Furthermore, these anti-jamming methods deal with mutual orthogonal waveforms. However, it is a difficult challenge to generate perfectly orthogonal waveforms for all Doppler and delay pairs in practice [37].

A further problem, due to the pseudo-random time delay in the FTG, is that the jamming is no longer independent and identically distributed (IID), which can induce severe performance degradation in the FDA-MIMO radar. Thus, it is essential that we tackle the problem of nonhomogeneous sample selection. The jamming-plus-noise covariance matrix is usually estimated with training data (called the secondary sample data) collected from the adjacent range bins. In practical scenarios, it is difficult to find enough secondary data of false targets since the presence of the false targets is unpredictable. Thus, the jamming-plus-noise covariance matrix cannot be precisely estimated due to the lack of IID training samples [38]. In order to solve this problem, traditional sample selection strategies based on the inner product [39], the generalized inner product (GIP) [40]–[42], the SMI test statistic [43], and the direct data domain (DDD) approach [44] were employed to remove bad samples and make a more precise estimation of the covariance matrix. On the other hand, the calculated weight vector applied to the data may cause target cancellation because of the presence of the desired target within the secondary sample data, which can severely degrade the performance of the adaptive matched filtering [45]. The robust DDD approach was suggested to solve this problem [46], [47], and there is scope to expand this approach of non-homogeneous sample selection to robust beamforming in the nonhomogeneous environments.

B. CONTRIBUTIONS

In this paper, an approach to suppress the main-beam deceptive jamming is studied in the FDA-MIMO radar using non-homogeneous sample detection. In particular, compared with the existing deceptive jamming suppression methods in the FDA-MIMO radar, the realistic case of non-perfectly orthogonal waveforms is considered.

The main contributions of this paper are given as follows.

1. Multiple false targets generated by the FTG have diverse range frequencies after time delay. Compared with the traditional pulse agility-based techniques performed in traditional radars, we use the FDA-MIMO radar which provides extra DOFs in the range domain. Based on this observation, in the presence of the range ambiguity and with a priori knowledge of the target, the difference of range ambiguity numbers (the number of pulses that the target spans) and the principal range values within an identical unambiguous range region can be used to discriminate the true and false targets. In this work, the transmit spatial frequency is compensated with the principal range value of the target. With the proposed

method, the true and false targets are distinguished in the joint transmit-receive spatial frequency domain.

2. Because the IID hypothesis for false targets is invalid due to pseudo-random time delay in the FTG, the suppression performance degrades. To obtain the jamming-plus-noise covariance matrix with high accuracy, a robust nonhomogeneous sample detection (NSD) method is proposed which includes two steps, i.e., 1) selecting the nonhomogeneous samples including signal and/or jamming; 2) rejecting the samples including signal according to the information of the signal of interest (SOI). As a result, the main-beam deceptive jamming can be suppressed due to the range mismatch through SOI pre-cancellation based robust two-dimensional (2-D) beamforming in transmit and receive dimensions.

C. PAPER ORGANIZATION

The remainder of this paper is organized as follows. Section II presents the signal model of the FDA-MIMO radar with the deceptive jamming. An approach to suppress the main-beam deceptive jamming with the FDA-MIMO radar is explored in Section III. Simulation results and performance analysis are given in Section IV. Conclusions are drawn in Section V.

II. SIGNAL MODEL OF FDA-MIMO RADAR WITH DECEPTIVE JAMMING

A. TRANSMITTED SIGNAL MODEL

Without loss of generality, we consider a colocated FDA-MIMO radar consisting of M half-wavelength spaced transmit elements and N receive elements in an identical uniform linear array. A small frequency increment Δf is introduced in the transmit array with the first element being the reference element. Thus, the carrier frequency fed to the m-th element is assigned as

$$f_m = f_0 + (m-1)\Delta f, \quad m = 1, 2, \cdots, M, \tag{1}$$

where f_0 is the reference carrier frequency. Each element transmits a phase-coded pulse which is composed of P subpulses and the transmitted signal of the m-th element can be expressed as

$$s_m(t) = \sqrt{\frac{E}{M}} x_m(t) e^{j2\pi f_m t}, \quad 0 \le t \le T_p, \tag{2}$$

where E is the total transmitted energy, t is the time within the radar pulse and T_p is the radar pulse duration and the signal's complex envelope $x_m(t)$ is expressed in the baseband as

$$x_m(t) = \sum_{l=1}^{P} \varphi_m(l) u[\frac{t-(l-1)\tau_b}{\tau_b}], \quad l = 1, 2, \cdots, P, \tag{3}$$

where $u(t) = \begin{cases} 1, \le t \le T_p \\ 0, else, \end{cases}$ τ_b is the length of each subpulse with $\tau_b = \frac{T_p}{P}$ and $\varphi_m(l)$ is the phase code to be designed, which can be expressed as

$$\varphi_m(l) = e^{j\phi_m(l)}, \tag{4}$$

where $\phi_m(l) \in [0, 2\pi]$ is the phase of the l-th of the m-th element. The phase value of the array can be concisely represented with the following $M \times P$ phase matrix:

$$\Phi = \begin{bmatrix} \boldsymbol{\varphi}_1 \\ \boldsymbol{\varphi}_2 \\ \vdots \\ \boldsymbol{\varphi}_M \end{bmatrix} = \begin{bmatrix} e^{j\phi_1(1)}, e^{j\phi_1(2)}, \cdots, e^{j\phi_1(P)} \\ e^{j\phi_2(1)}, e^{j\phi_2(2)}, \cdots, e^{j\phi_2(P)} \\ \vdots \\ e^{j\phi_M(1)}, e^{j\phi_M(2)}, \cdots, e^{j\phi_M(P)} \end{bmatrix}, \tag{5}$$

where $\boldsymbol{\varphi}_m = [\varphi_m(1), \varphi_m(2), \cdots, \varphi_m(P)]_{1\times P}$ represents the polyphase sequence transmitted by the m-th element. The optimization of the discrete waveform set $\{\varphi_m(l)\}_{m=1,l=1}^{M,P}$ with desired correlation properties can be achieved by the CAN algorithm [48], summarized in Algorithm 1.

Algorithm 1 The CAN Algorithm Proposed in [48]

Require: sequence length P

1. Set iteration number $k = 0$ and initialize $\boldsymbol{\varphi}_m^{(0)}$;
2. Transform $\boldsymbol{\varphi}_m^{(k)}$ to the frequency domain $\boldsymbol{\varphi'}_m^{(0)}$ via fast Fourier transform (FFT);
3. Compute $v_i = e^{j\arg \boldsymbol{\varphi'}_m^{(0)}}$, $i = 1, 2, \cdots, 2P$;
4. Transform v to the time domain via inverse fast Fourier transform (IFFT);
5. Compute $\boldsymbol{\varphi}_m^{(k+1)} = e^{j\arg v'_i}$, $i = 1, 2, \cdots, P$;
6. Repeat 2∼5 until pre-specified stop criterion is satisfied.

Output: the waveform matrix Φ.

B. RECEIVED SIGNAL MODEL

For a target located in the far-field at the angle θ_0 and range R_0, the demodulated baseband signal which is transmitted by the m-th element and then received by the n-th ($n = 1, 2, \cdots, N$) element can be expressed as

$$\begin{aligned} y_{m,n}(t-\tau_{m,n}) &= \beta x_m(t-\tau_{m,n}) e^{j2\pi f_m(t-\tau_{m,n})} \\ &\approx \beta x_m(t-\tau_0) e^{j2\pi f_m(t-\tau_{m,n})}, \end{aligned} \tag{6}$$

where $\tau_{m,n} = \frac{2R_0 - d(n-1)\sin(\theta_0) - d(m-1)\sin(\theta_0)}{c}$ is the round-trip propagation time delay, β is the complex-valued coefficient of the point source, d is the inter-element spacing, and c is the speed of light. The narrowband assumption is assumed, i.e., $x_m(t-\tau_{m,n}) \approx x_m(t-\tau_0)$ and $\tau_0 = \frac{2R_0}{c}$ is the common time delay. Note that the Doppler effect is neglected here.

The signal received by the n-th element can be expressed as

$$\begin{aligned} y_n(t, \theta_0) \approx \beta e^{j2\pi f_0(t-\tau_0)} \sum_{m=1}^{M} x_m(t-\tau_0) e^{j2\pi \Delta f(m-1)(t-\tau_0)} \\ \cdot e^{j2\pi \frac{d}{\lambda_0}(m-1)\sin(\theta_0)}, \end{aligned} \tag{7}$$

where $\lambda_0 = \frac{c}{f_0}$ is the wavelength.

It is assumed that the false targets are generated by the FTG and they are usually the time-delayed replicas of the captured waveform. We consider a FTG positioned at the angle θ_j and

range R_j. Thus, the corresponding waveform received by the n-th element is

$$J_n(t) = \sum_{q=1}^{Q}\sum_{m=1}^{M} \beta_q \varphi_m(t-\tau_j-\tau_q)e^{j2\pi f_m(t-\tau_j-\tau_q)}, \quad (8)$$

where β_q is the complex-valued coefficient of the q-th ($q = 1, 2, \cdots, Q$) false target, Q is the number of false targets, $\tau_j = \frac{2R_j - d(n-1)\sin(\theta_j) - d(m-1)\sin(\theta_j)}{c}$ is the round-trip propagation time delay between the nth element and the FTG, and τ_q is the time delay corresponding to the q-th false target in the FTG. In particular, the FTG can create a false target with an apparent negative range offset by delaying the stored pulse until a fixed time before the next incoming radar pulse [34]. For the q-th false target, the received signal by the n-th element after demodulation can be written as

$$\begin{aligned} J_{q,n,m} \approx{}& \beta_q e^{j2\pi f_0\left(t-\left(\frac{2R_j}{c}+\tau_q\right)\right)} e^{j2\pi\frac{d}{\lambda_0}(n-1)\sin(\theta_j)} \\ &\cdot \sum_{m=1}^{M} x_m(t-\tau_0) e^{j2\pi\Delta f(m-1)\left(t-\left(\frac{2R_j}{c}+\tau_q\right)\right)} e^{j2\pi\frac{d}{\lambda_0}(m-1)\sin(\theta_j)} \end{aligned} \quad (9)$$

where $\frac{2R_j}{c}+\tau_q$ represents the time delay corresponding to the actual position of the q-th false target, which can be written as $\frac{2R_q}{c}$, where R_q is the actual position of the q-th false target. The time delay in FTG makes it possible to settle the false targets in both negative and positive range offsets [6].

Subsequently, the received signals are down-converted, matched filtered and stored. And the received signal from each receive element can be decomposed by M matched filters, yielding M waveforms [49], which is shown in Fig. 1.

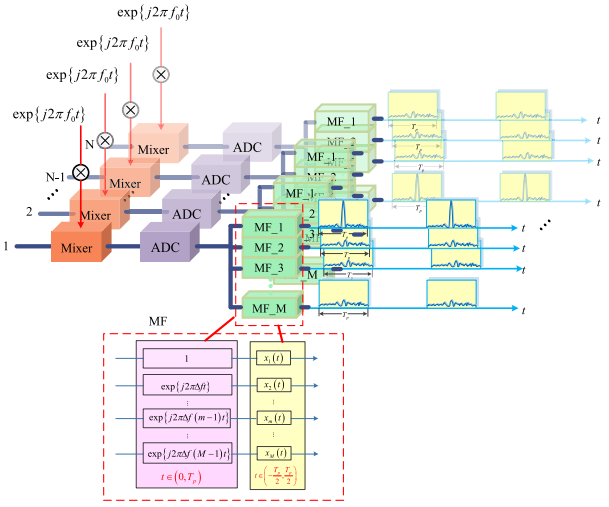

FIGURE 1. Signal processing at the receiver with multiple match-filtered waveforms.

Due to the incremental frequency, an extra number of range-dependent DOFs is provided and the range-angle-dependent transmit steering vector $\mathbf{a}(R,\theta) \in \mathbb{C}^{M\times 1}$ can be written as

$$\begin{aligned} \mathbf{a}(R_0,\theta_0) &= \mathbf{a}(R_0)\odot\mathbf{a}(\theta_0) \\ &= \left[1, e^{-j4\pi\frac{\Delta f}{c}R_0}, \cdots, e^{-j4\pi\frac{\Delta f}{c}(M-1)R_0}\right]^{\mathrm{T}} \\ &\odot \left[1, e^{j2\pi\frac{d}{\lambda_0}\sin(\theta_0)}, \cdots, e^{j2\pi\frac{d}{\lambda_0}(M-1)\sin(\theta_0)}\right]^{\mathrm{T}}, \end{aligned} \quad (10)$$

where $\odot$ is the Hadamard product and $^{\mathrm{T}}$ denotes the transpose operator. It can be seen that the range information of the target is contained in the transmit steering vector. And the angle-dependent receive steering vector $\mathbf{b}(\theta) \in \mathbb{C}^{N\times 1}$ has the form of

$$\mathbf{b}(\theta) = \left[1, e^{j2\pi\frac{d}{\lambda_0}\sin(\theta)}, \cdots, e^{j2\pi\frac{d}{\lambda_0}(N-1)\sin(\theta)}\right]^{\mathrm{T}}. \quad (11)$$

However, due to hardware limitations, the mutual orthogonality among the received signals cannot be achieved in practice for all Doppler and delay pairs. Thus, the waveforms cannot be exactly separated because of their imperfect mutual orthogonality. For simplicity, by stacking the output vector of all N receive channels, the received signal of the target can be represented in a simple form

$$\mathbf{x}_{\mathrm{S}} = \zeta_{\mathrm{S}}\mathbf{b}(\theta_0)\mathbf{a}^{\mathrm{T}}(R_0,\theta_0)\Phi, \quad (12)$$

where ζ_{S} denotes the equivalent coefficient of the target. Similarly, the received signal of the q-th false target can also be represented as

$$\mathbf{x}_q = \zeta_q\mathbf{b}_{\mathrm{J}}(\theta_j)\mathbf{a}_{\mathrm{J}}^{\mathrm{T}}(R_q,\theta_j)\Phi, \quad (13)$$

where ζ_q denotes the equivalent coefficient of the q-th false target, $\mathbf{a}_{\mathrm{J}}(R_q,\theta_j) \in \mathbb{C}^{M\times 1}$ and $\mathbf{b}_{\mathrm{J}}(\theta_j) \in \mathbb{C}^{N\times 1}$ denote the transmit and the receive steering vector of the q-th false target, respectively.

As a result, all the received signal vector of the FDA-MIMO radar can be obtained as in equation (14)

$$\begin{aligned} \mathbf{x} &= \mathbf{x}_{\mathrm{S}} + \sum_{q=1}^{Q}\mathbf{x}_q + \mathbf{n} \\ &= \zeta_{\mathrm{S}}\mathbf{b}(\theta_0)\mathbf{a}^{\mathrm{T}}(R_0,\theta_0)\Phi + \sum_{q=1}^{Q}\zeta_q\mathbf{b}_{\mathrm{J}}(\theta_j)\mathbf{a}_{\mathrm{J}}^{\mathrm{T}}(R_q,\theta_q)\Phi + \mathbf{n}, \end{aligned} \quad (14)$$

where $\mathbf{x}_{\mathrm{S}}$, $\sum_{q=1}^{Q}\mathbf{x}_q$ and $\mathbf{n}$ denote the true target, deceptive jamming and noise components, respectively. And the output vector of the signal after matched filtering can be represented as in equation (15)

$$\begin{aligned} \mathbf{y} = {}& \alpha_0\mathbf{b}(\theta_0)\otimes\mathbf{R}_{\mathrm{S}}\mathbf{a}(R_0,\theta_0) \\ &+ \sum_{q=1}^{Q}\alpha_q\mathbf{b}_{\mathrm{J}}(\theta_j)\otimes\mathbf{R}_{\mathrm{S}}\mathbf{a}_{\mathrm{J}}(R_q,\theta_j) + \mathbf{v}, \end{aligned} \quad (15)$$

where $\otimes$ denotes the Kronecker product, $\mathbf{R}_{\mathrm{S}} = E\{\Phi\Phi^{\mathrm{H}}\}/M$ is waveform covariance matrix, denotes the conjugate transpose operator and $\mathbf{v} = E\{\mathbf{n}\Phi^{\mathrm{H}}\}/M$.

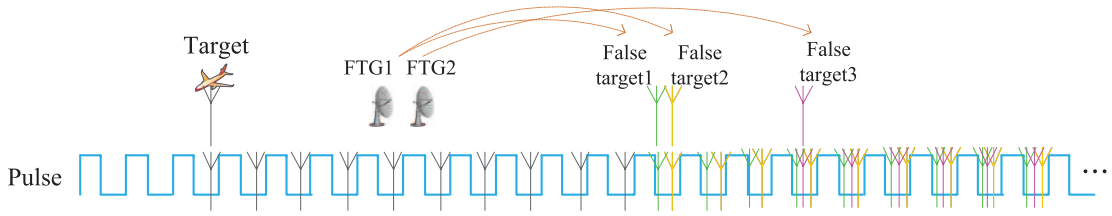

FIGURE 2. Generation of the deceptive jamming.

III. MAIN-BEAM DECEPTIVE JAMMING SUPPRESSION APPROACH

In this section, an approach to suppress the main-beam deceptive jamming with the FDA-MIMO radar is explored. Firstly, the principle of the main-beam deceptive jamming discrimination in the FDA-MIMO is studied. Next, a robust NSD method is proposed to precisely estimate the jamming-plus-noise covariance matrix. Finally the procedure of deceptive jamming suppression approach using NSD is derived.

A. DECEPTIVE JAMMING DISCRIMINATION

In practice, it requires several pulse repetition intervals (PRIs) for the FTG to intercept and decode the operating parameters of the radar's transmitted waveform. Then, multiple false targets are generated by the FTG and they are usually time delayed replicas of the captured waveform. It is known that the false targets in side-lobes can be suppressed. In contrast, the main-beam deceptive jamming is very challenging to be mitigated effectively in the traditional radar framework. To solve this problem, the range information is exploited in the FDA-MIMO radar thanks to the extra range-dependent DOFs provided by this radar approach.

Generally, the position of the target is coarsely estimated in the radar searching stage. Afterwards, in the radar tracking stage, assume the location information of the target is known. It follows from (10) and (11) that the corresponding transmit and receive spatial frequencies of the true target can be expressed as

$$f_{\mathrm{T}} = -\Delta f \frac{2R_0}{c} + \frac{d}{\lambda_0}\sin(\theta_0), \tag{16a}$$

$$f_{\mathrm{R}} = \frac{d}{\lambda_0}\sin(\theta_0). \tag{16b}$$

Similarly, the corresponding transmit and receive spatial frequencies of the q-th false target generated by the FTG are respectively expressed as

$$f_{\mathrm{T}q} = -\Delta f \frac{2R_q}{c} + \frac{d}{\lambda_0}\sin(\theta_j), \tag{17a}$$

$$f_{\mathrm{R}q} = \frac{d}{\lambda_0}\sin(\theta_j). \tag{17b}$$

It can be seen from (16) and (17) that the transmit spatial frequency is range-angle-dependent. Hence, the target can be arbitrarily distributed in the joint transmit-receive spatial frequency domain.

In high pulse repetition frequency (PRF) case, range ambiguity arises. In such case, the range of the target is written as

$$R_0 = r_0 + (p-1)R_u, \tag{18}$$

where r_0 is the principal range of the target, which can be determined by the number of range bins and size of the range bin, $R_u = \frac{c}{2f_r}$ is the maximum unambiguous range, and $p = \mathrm{int}\left(\frac{R_0}{R_u}\right)$ is the range ambiguity number of the target (the number of pulses that the target spans), where int$(\cdot)$ denotes the operator that rounds to the nearest integer less than or equal to that number. We have $p \in [1, N_a]$, where N_a denotes the number of ambiguous ranges. Assume that the FTG requires several PRIs to simulate the intercepted waveform, and the range of the q-th false target is written as

$$R_q = r_q + (p'-1)R_u, \tag{19}$$

where r_q is the principal range of the q-th false target and $p' = \mathrm{int}\left(\frac{R_q}{R_u}\right)$ is the range ambiguity number of the q-th false target.

Fig.2 gives an illustration of the generation of deceptive jamming. It is assumed that the false target 1 and the false target 2 are generated by the FTG 1, and the false target 3 is generated by the FTG 2. It is obvious that due to the difference of principal range values within an identical unambiguous range region, the false target 1, the false target 3 and the true target are easily to identify. However, the false target 2 and the true target have the identical principal range value. Thus, the difference of range ambiguity numbers make it possible to discriminate the true and false target.

For a fixed angle, the spatial frequency difference between two point targets distanced by R_u can be expressed as

$$\Delta f_{\mathrm{diff}} = \frac{2\Delta f}{c}R_u = \frac{\Delta f}{f_r} = z + \nu, \tag{20}$$

where $z = \mathrm{int}\left(\frac{\Delta f}{f_r}\right)$ is an integer part and $\nu \in [0, 1)$ is the decimal part. Note that z and ν are constant scalars once Δf and f_r are given. Due to the 2π periodicity of the phase difference, the principal value of the spatial frequency only occupies $[-0.5, 0.5]$. Thus, the influence of z is ignored.

Fig. 3 shows the spectrum distribution of the target in the presence of range ambiguity in the FDA-MIMO radar with $N_a = 4, k = 0, 1, 2, \cdots$. It is observed that the spectrum distribution of the target is distinguishable for

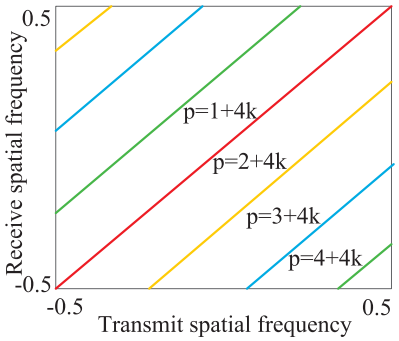

FIGURE 3. The spectrum distribution of the target in the presence of range ambiguity.

different ambiguous ranges. Moreover, the range ambiguous echoes spread in the spatial frequency domain without overlap.

As the principal range can be determined, the range frequency corresponding to the principal range can be compensated range-by-range [33]. After compensating with $f_C = \frac{2r_0\Delta f}{c}$, the transmit spatial frequency of the true target and the q-th false target are respectively expressed as

$$\tilde{f}_T = f_T + f_C = -(p-1)\nu + \frac{d}{\lambda_0}\sin(\theta_0), \tag{21a}$$

$$\tilde{f}_F = f_{Tq} + f_C = \frac{2r_\Delta \Delta f}{c} - (p'-1)\nu + \frac{d}{\lambda_0}\sin(\theta_j), \tag{21b}$$

where $r_\Delta = r_0 - r_q$ is the surplus principal range after compensation. Hence, the true and false targets are distinguishable as they belong to different range regions.

It is shown in Fig.4 that after compensation, the true and false targets are distinguishable in the transmit spatial frequency domain. Usually, the power of the false target is larger than the true target. Thus, the deceptive jamming can be discriminated.

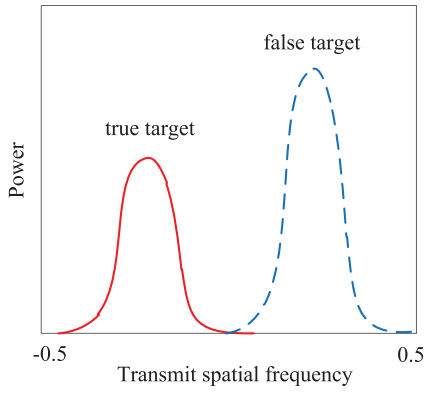

FIGURE 4. An example of the spectrum in the transmit spatial frequency domain.

For main-beam deceptive jamming, i.e., $\theta_0 = \theta_j$, the difference of transmit spatial frequency between the true and false targets is calculated as

$$\begin{aligned}\Delta\tilde{f} &= \left|\tilde{f}_T - \tilde{f}_F\right| \\ &= \left|(p'-p)\nu - \frac{2r_\Delta \Delta f}{c}\right|.\end{aligned} \tag{22}$$

Note that, the FTG tries to reradiate the replicas, i.e., the false targets, as rapidly as possible. However, it usually requires several PRIs to intercept the radarąŕs operating parameters. Without loss of generality, we assume the maximum time delay in the FTG is smaller than $N_a \times$PRIs. Considering the maximum time delay within the FTG, we have $p' = p + N_a$. As the surplus principal range r_Δ is smaller than the range bin size, it is reasonable to ignore the influence of $\frac{2r_\Delta \Delta f}{c}$ in analyzing the difference of transmit spatial frequency $\Delta\tilde{f}$. Note that the delayed number of pulses corresponding to the false targets can be any values smaller than N_a. Thus, $\Delta\tilde{f}$ should be smaller than 1 to avoid periodical aliasing. It is obtained that the condition $\nu < \frac{1}{N_a}$ holds and the targets can be distinguishable in the transmit frequency.

B. DECEPTIVE JAMMING SUPPRESSION

Subsequently, the received signals are processed through a transmit-receive 2-D beam-former. The minimum variance distortionless response (MVDR) beam-former is used which is mathematically equivalent to the following convex optimization problem

$$\min_{\mathbf{w}} \left\{\mathbf{w}^H \mathbf{R}_{j+n} \mathbf{w}\right\} \quad \text{s.t. } \mathbf{w}^H \mathbf{u}(R_0, \theta_0) = 1, \tag{23}$$

where $\mathbf{R}_{j+n}$ denotes the jamming-plus-noise covariance matrix, $\mathbf{u}(R_0, \theta_0)$ denotes the virtual steering vector of the FDA-MIMO radar, i.e., $\mathbf{u}(R_0, \theta_0) = \mathbf{b}(\theta_0) \otimes \mathbf{a}(R_0, \theta_0)$, $\mathbf{w} = \mu \mathbf{R}_{j+n}^{-1} \mathbf{u}(R_0, \theta_0)$ is the $MN \times 1$ optimal weight vector, $\mu = \frac{1}{\mathbf{u}(R_0,\theta_0)^H \mathbf{R}_{j+n}^{-1} \mathbf{u}(R_0,\theta_0)}$.

As a result, the main-beam deceptive jamming can be suppressed because of the range mismatch. The flow chart of the suppression algorithm for the main-beam deceptive jamming with the FDA-MIMO radar is shown in Fig. 5.

In practice, the sampled covariance matrix is usually adopted instead of the population covariance matrix because the latter is unknown. Typically, the sample covariance matrix is determined using the secondary sample data from range bins close to the range bin under test [38]. However, this is not possible in deceptive jamming suppression task. Because of the random time-delay in FTG, the IID condition cannot be satisfied for the false targets. Therefore, the training samples should be selected to precisely estimate the jamming-plus-noise covariance matrix.

Let $\mathbf{X}$ denotes the radar signal sample at the ℓ-th ($\ell = 1, 2, \cdots, L$) range bin and k-th ($k = 1, 2, \cdots, K$) pulse, where L is the number of range bins and K is the number of pulses in one coherent processing interval. Thus, the target detection issue can be formulated as a quaternary hypothesis

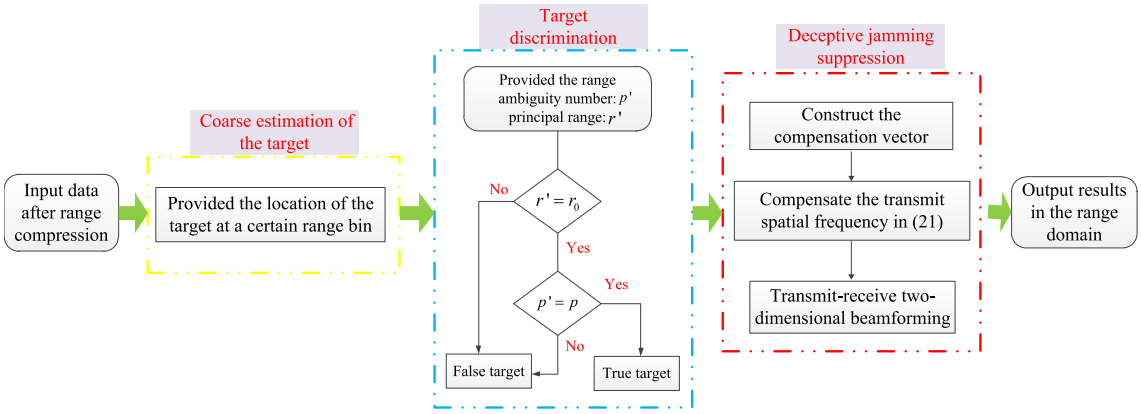

FIGURE 5. Flow chart of the main-beam deceptive jamming suppression approach with the FDA-MIMO radar.

testing problem, that is

$$\begin{cases} H_0 : \mathbf{X} = \mathbf{N} \\ H_1 : \mathbf{X} = \mathbf{J} + \mathbf{N} \\ H_2 : \mathbf{X} = \mathbf{S} + \mathbf{N} \\ H_3 : \mathbf{X} = \mathbf{S} + \mathbf{J} + \mathbf{N}, \end{cases} \tag{24}$$

where $\mathbf{S}$, $\mathbf{J}$ and $\mathbf{N}$ represent the $MN \times K \times L$ matrices of the true target, false targets and noise, respectively, which are collected in three dimensions, i.e., transmit-receive element, pulse and range bin.

Note that the false targets $\mathbf{J}$ can be arbitrarily settled in any range bin to confuse the radar, and the true target $\mathbf{S}$ can be distributed in different range bins from false targets which refers to the H_2 hypothesis, or in an identical range bin with a false target which refers to the H_3 hypothesis. Thus, the issue of true target detection can be formulated as a selection between H_2/H_3. In order to precisely estimate the jamming-plus-noise covariance matrix, the expected samples which are under the H_1 hypothesis should be selected. Therefore, we resort to a robust NSD method which includes two steps, i.e., 1) selecting the nonhomogeneous samples including signal and/or jamming; 2) rejecting the samples including signal according to the information of the SOI. The steps will be discussed as follows.

Step 1 (Nonhomogeneous Samples Selection): In the first step, the samples belong to H_1 and H_2/H_3 are detected, which denotes the adaptive NSD method. Note that they are different from the H_0 hypothesis as they contain large power components, i.e., the signal or jamming. Given a range bin, the data matrix in element and pulse dimensions is utilized to calculate the covariance matrix. The secondary sample data is collected in pulse dimension here and we obtain the covariance matrix as

$$\hat{\mathbf{R}}_\ell = \frac{1}{K} \sum_{k=1}^{K} \tilde{\mathbf{x}}_{k,\ell} \tilde{\mathbf{x}}_{k,\ell}^{\mathrm{H}}, \tag{25}$$

where $\tilde{\mathbf{x}}_{k,\ell}$ is the snapshot in the transmit-receive dimension corresponding to the k-th pulse and the ℓ-th range bin.

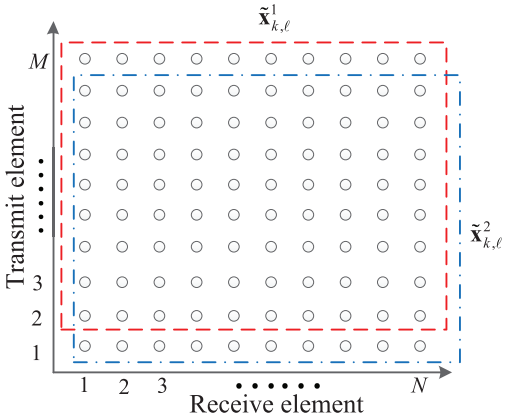

FIGURE 6. Spatial cancellation based on the information of the SOI.

Thus, the energy of data corresponding to the ℓ-th range bin can be estimated as

$$P_{\mathbf{X}} = \mathrm{trace}\left(\hat{\mathbf{R}}_\ell\right). \tag{26}$$

It is assumed that the energy of the nonhomogeneous sample data, namely the data containing signal and/or jamming, is above the threshold which is determined according to the probability distribution function of noise and false alarm ratio, that is,

$$\eta = F\left(P_f | H_0\right), \tag{27}$$

where P_f denotes the false-alarm ratio. Given the assumption of white Gaussian distributed noise with zero mean and variance σ_n^2, i.e., $\mathbf{n} \sim CN\left(\mathbf{0}, \sigma_n^2 \mathbf{I}_{M\times N}\right)$, $\mathbf{I}_{M\times N}$ is a $M \times N$ matrix with all elements being one, the false alarm ratio can be determined as follows [50]

$$P_f = \int_\eta^\infty \frac{r}{\sigma_n^2} \exp\left(\frac{-r^2}{2\sigma_n^2}\right). \tag{28}$$

Thus, for a given false-alarm ratio, the threshold can be calculated as

$$\eta = \sqrt{2\sigma_n^2 \ln\left(\frac{1}{P_f}\right)}. \tag{29}$$

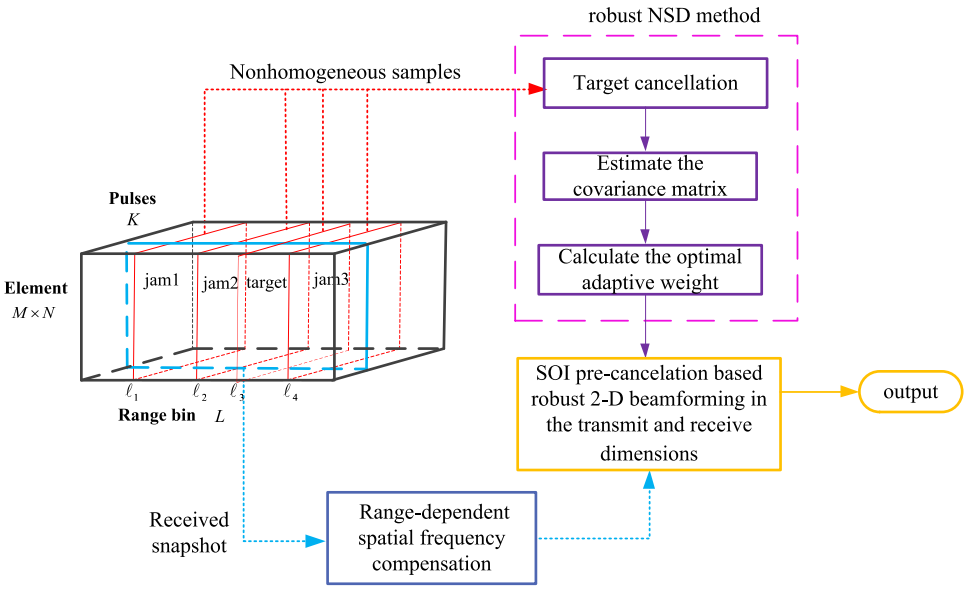

FIGURE 7. The process of deceptive jamming suppression using robust NSD method with FDA-MIMO radar.

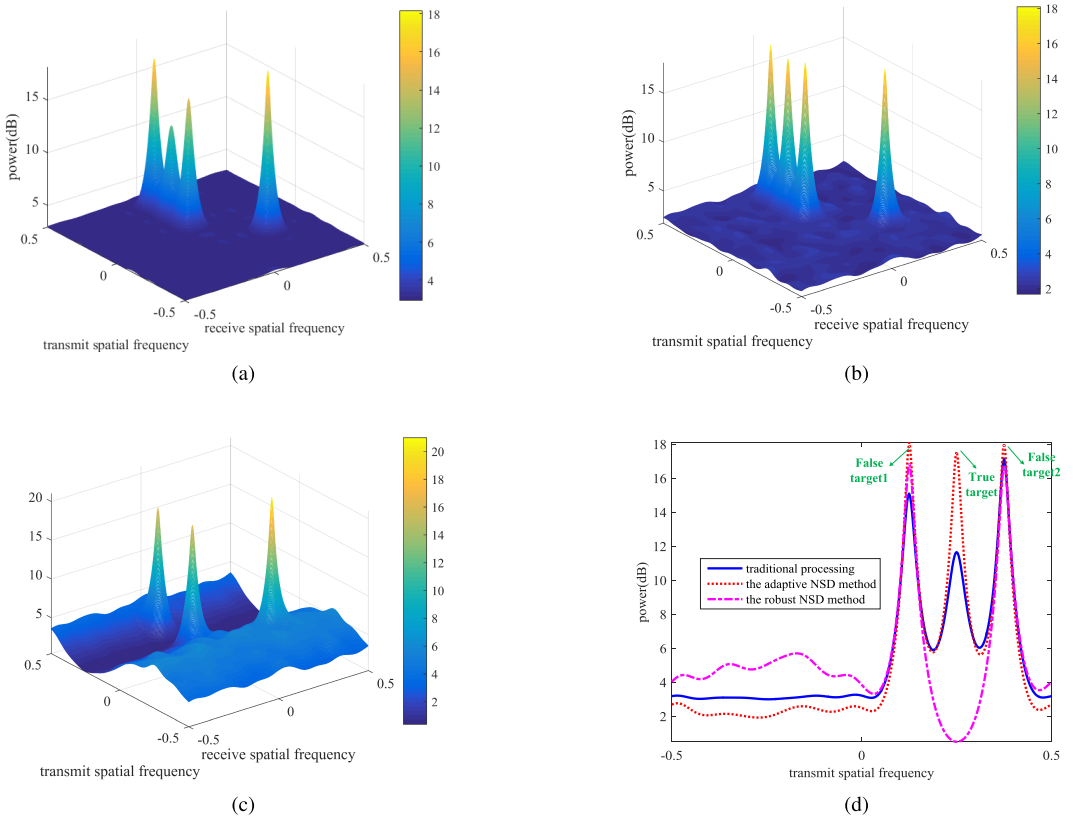

FIGURE 8. Capon spectrum distributions of the true target and false targets with the FDA-MIMO radar. (a) The Capon spectrum with traditional processing; (b) The Capon spectrum with the adaptive NSD method; (c) The Capon spectrum with the robust NSD method; (d) Comparison of sample selection strategies.

It should be emphasized that a relatively high false alarm ratio is utilized in the first step to choose the samples containing signal and/or jamming. This is because the selected samples are used to estimate the covariance matrix, hence all samples with large power components should be selected.

TABLE 1. Simulation parameters of FDA-MIMO radar.

Parameter	Value	Parameter	Value	Parameter	Value
Number of elements	10	Carrier frequency	10 GHz	Wavelength	0.03 m
Bandwidth	20 MHZ	Frequency increment	251250 Hz	PRF	5000 Hz
Number of pulses	30	Number of range bins	200	Range of the target	110 km
Angle of the target	0°	Range of the false target1	245 km	Angle of the false target1	0°
Range of the false target2	255 km	Angle of the false target2	0°	Range of the false target3	265 km
Angle of the false target3	30°				

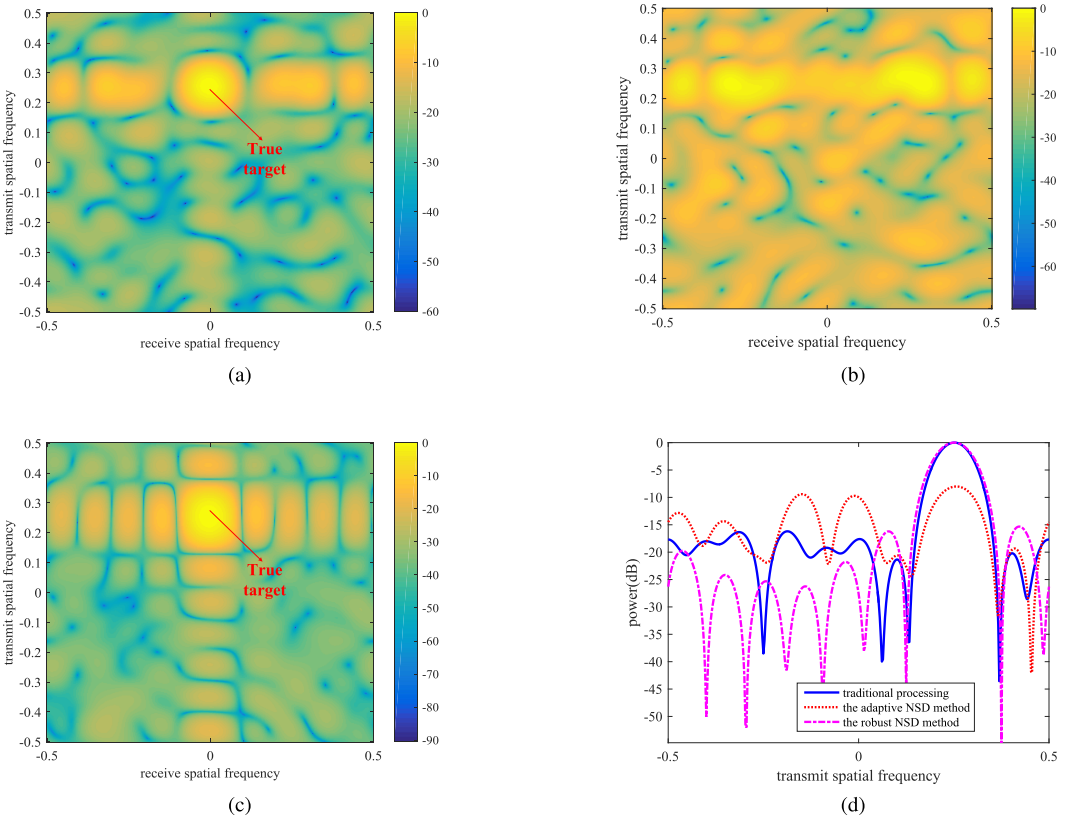

FIGURE 9. The adaptive beam-pattern results of the FDA-MIMO radar. (a) The beam-pattern with traditional processing; (b) The beam-pattern with the adaptive NSD method; (c) The beam-pattern with the robust NSD method; (d) Comparison of sample selection strategies.

After the first step, the samples belonging to H_1 and H_2/H_3 hypotheses are selected, i.e., the adaptive NSD method.

Step 2 (SOI Cancellation): The presence of the target within the secondary sample data severely can degrade the performance of the matched filter. Therefore, the SOI should be avoided. In the second step, the spatial cancellation based on the information of the SOI is performed by smoothing once in the joint transmit-receive domain. As depicted in Fig. 6, in this procedure, the $\overset{\sim}{\mathbf{x}}_{k,\ell}$ is divided into two matrices in the transmit-receive dimension, that is, the matrix $\overset{\sim}{\mathbf{x}}^{1}_{k,\ell}$ contains the former $M-1$ transmit elements and the matrix $\overset{\sim}{\mathbf{x}}^{2}_{k,\ell}$ contains the latter ones. Both of them have the dimension of $(M-1)\times N$. Subsequently, the SOI cancellation procedure is performed to exclude the possible target from the secondary sample data, that is,

$$\overset{\sim}{\mathbf{x}}^{0}_{k,\ell} = \overset{\sim}{\mathbf{x}}^{1}_{k,\ell} - \alpha^{-1}\overset{\sim}{\mathbf{x}}^{2}_{k,\ell}. \tag{30}$$

where $\alpha = \exp\{j2\pi\tilde{f}_{\mathrm{T}}\}$.

Hence, the re-constructed covariance matrix is calculated by adding $\overset{\sim}{\mathbf{x}}^{0}_{k,\ell}$ in each selected range bin under the H_1 hypothesis, that is

$$\overset{\sim}{\mathbf{R}} = \frac{1}{N_s}\sum_{\ell=1}^{N_s}\frac{1}{K}\sum_{k=1}^{K}\overset{\sim}{\mathbf{x}}^{0}_{k,\ell}\overset{\sim}{\mathbf{x}}^{0\ \mathrm{H}}_{k,\ell}, \tag{31}$$

where N_s is the number of the selected nonhomogeneous samples along the range bin. If the true and the false targets are in the same range bin, we have $N_s = Q$, otherwise, $N_s = Q+1$.

In the robust NSD method, the detector selects the nonhomogeneous samples including signal and/or jamming, and then rejects the samples including signal according to the information of the SOI. The method combines efficiency and reduced computational complexity, but may suffer of spatial resolution loss in the process of target cancellation based on spatial smoothing. In other words, the selection of effective training samples in the nonhomogeneous environments for

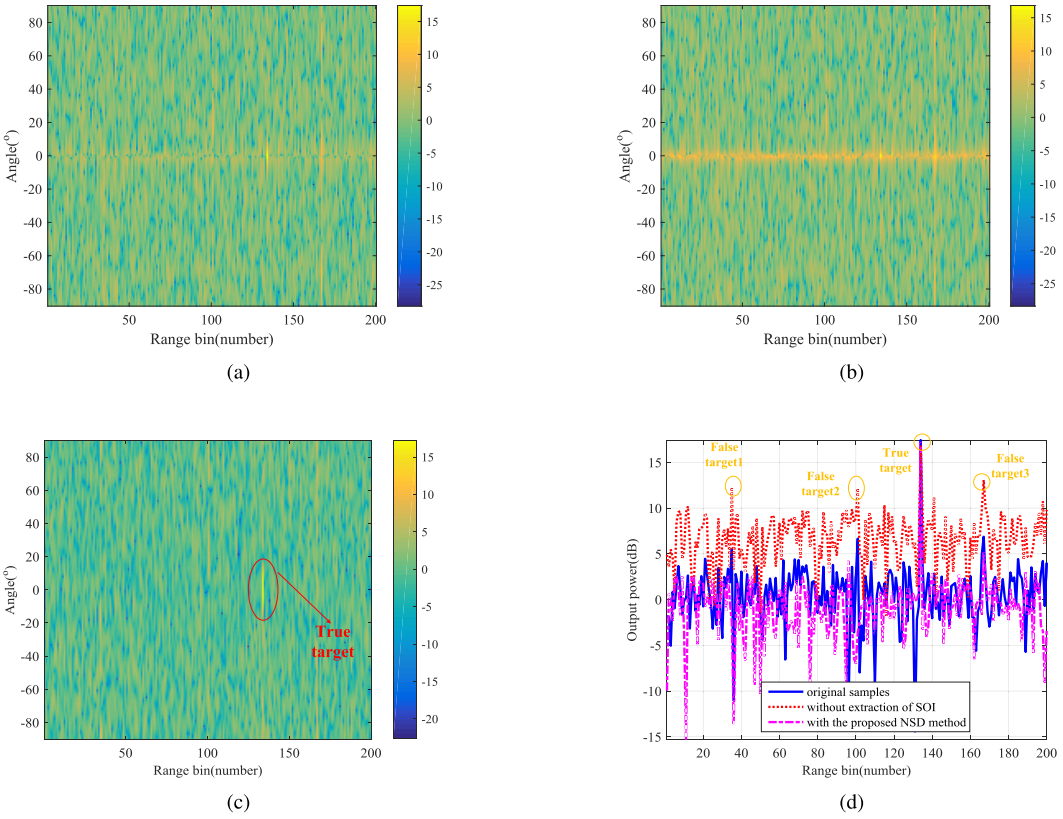

FIGURE 10. Output power of range-angle adaptive matched filter with the FDA-MIMO radar. (a) Output power with traditional processing; (b) Output power with the adaptive NSD method; (c) Output power with the robust NSD method; (d) Comparison of sample selection strategies.

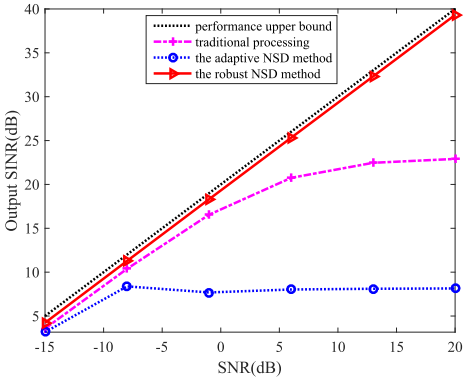

FIGURE 11. Output SINR versus input SNR performance for different sample selection strategies.

the robust NSD method is at the cost of reducing the effective aperture. Besides, the computational complexity of the proposed method is $O\left((MN)^3\right)$ owing to the calculation of the inverse covariance matrix.

As an illustrative example, the process of deceptive jamming suppression approach using the robust NSD method is provided in Fig.7. It is shown that the data cube represents the $MN \times K \times L$ complex baseband samples. Three range bins, i.e., ℓ_1, ℓ_2, and ℓ_4, are contaminated by the false targets, while the true target dwells at another range bin, i.e., ℓ_3. In the first step of the proposed method, it is desired that the nonhomogeneous samples, i.e., ℓ_1, ℓ_2, ℓ_3 and ℓ_4, are selected. In the second step, spatial smoothing is perform to cancel the target component in range bin ℓ_3. Thus, the jamming-plus-noise covariance matrix can be estimated accurately as the secondary sample data is approximately IID and the optimal adaptive weight of the MVDR beam-former can be achieved. Finally, the main-beam deceptive jamming can be suppressed in the joint transmit-receive domain through SOI pre-cancellation based robust 2-D beamforming in the transmit and receive dimensions, which results in performance improvement of the adaptive deceptive jamming suppression.

IV. SIMULATION RESULTS

In this section, simulations are performed to verify the effectiveness of the proposed deceptive jamming suppression approach with FDA-MIMO radar using nonhomogeneous sample detection. The simulation parameters are listed in Table 1.

In this simulation, we set $N_a = 4$ and $\Delta f = 251250$Hz. Thus, $z = 50$ and $\nu = 0.25$ are determined using (23). It is assumed that the FTG 1 is located in the main-beam and FTG 2 is located in the side-lobe. The false targets generated by the FTG 1 are at range bins 35 and 101, respectively. And the

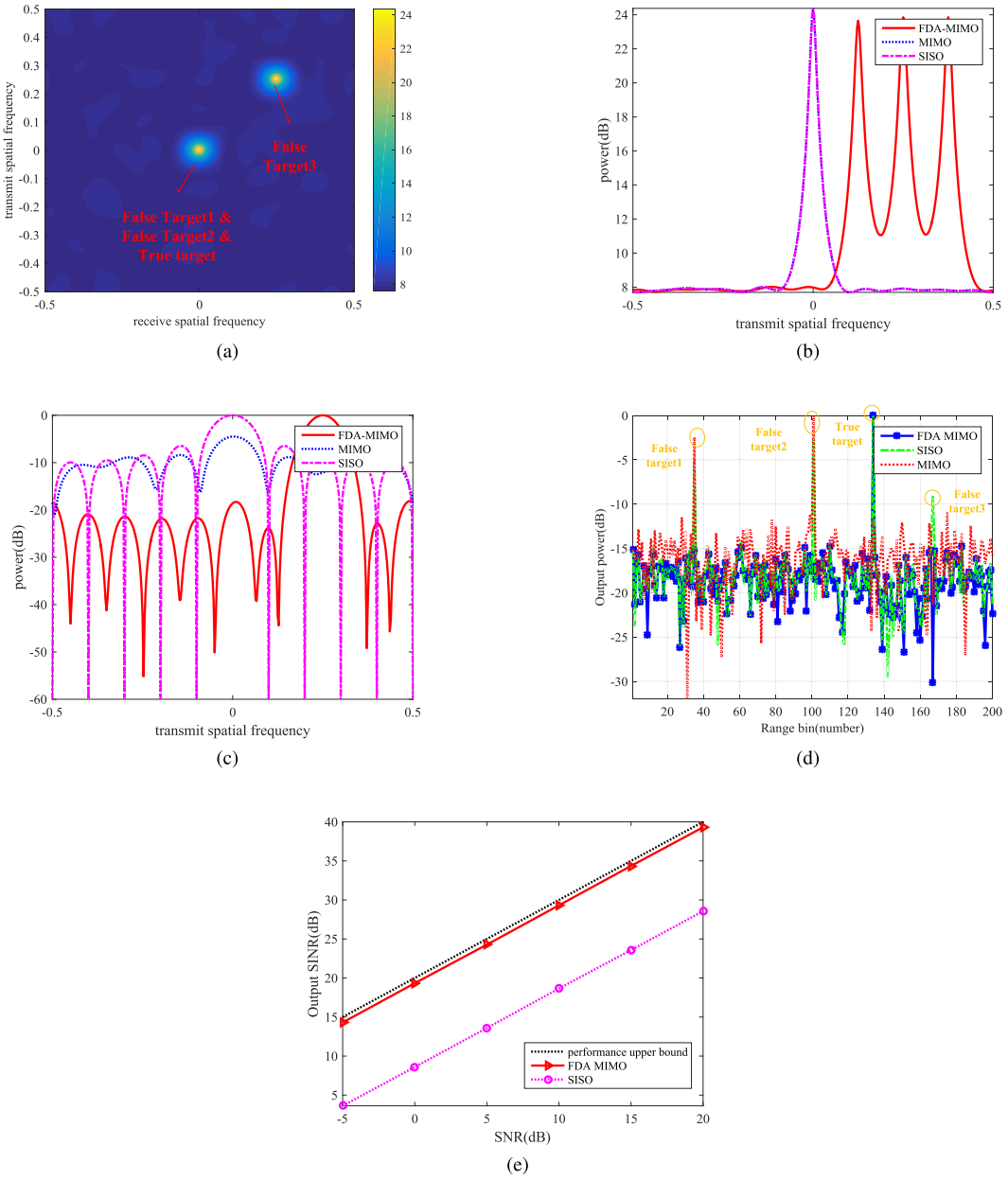

FIGURE 12. Comparison among different radar frameworks (a) Capon spectrum distribution of MIMO radar; (b) Capon spectrum distributions at $\theta_0 = 0°$; (c) Beam-patterns; (d) Output powers of range-angle adaptive matched filter; (e) Output SINR versus input SNR performance for different radar frameworks.

false target generated by the FTG 2 is at range bin 167. The index of the range bin for the target is 134.

A. DECEPTIVE JAMMING SUPPRESSION RESULTS WITH THE ROBUST NSD METHOD

In this subsection, the performance of deceptive jamming suppression in the FDA-MIMO radar with nonhomogeneous sample selection is investigated. In the presence of range ambiguity, the ambiguity number of the true target is 4 and the ambiguity numbers of the false targets equal 9. Fig. 8 shows the Capon spectrum distributions of the true and false targets in the joint transmit-receive spatial frequency domain. It is shown that after compensation, the spectrum distribution of the true and false targets are distinguishable thanks to the extra range-dependent DOFs introduced by the FDA-MIMO radar. Specifically, Fig. 8 (a), Fig. 8 (b) and Fig. 8 (c) respectively plot the spectra with the traditional processing without selecting the nonhomogeneous samples, the adaptive NSD method and the robust NSD method. As shown in Fig. 8 (d), in the plot with $f_R = 0$, the power of the target with the traditional processing decreases compared with the adaptive NSD method. Additionally, in the robust NSD method, the SOI is effectively extracted.

Fig. 9 demonstrates the adaptive range-angle-dependent beam-pattern results in the joint transmit-receive spatial frequency domain. As shown in Fig. 9 (a) and Fig. 9 (c), using

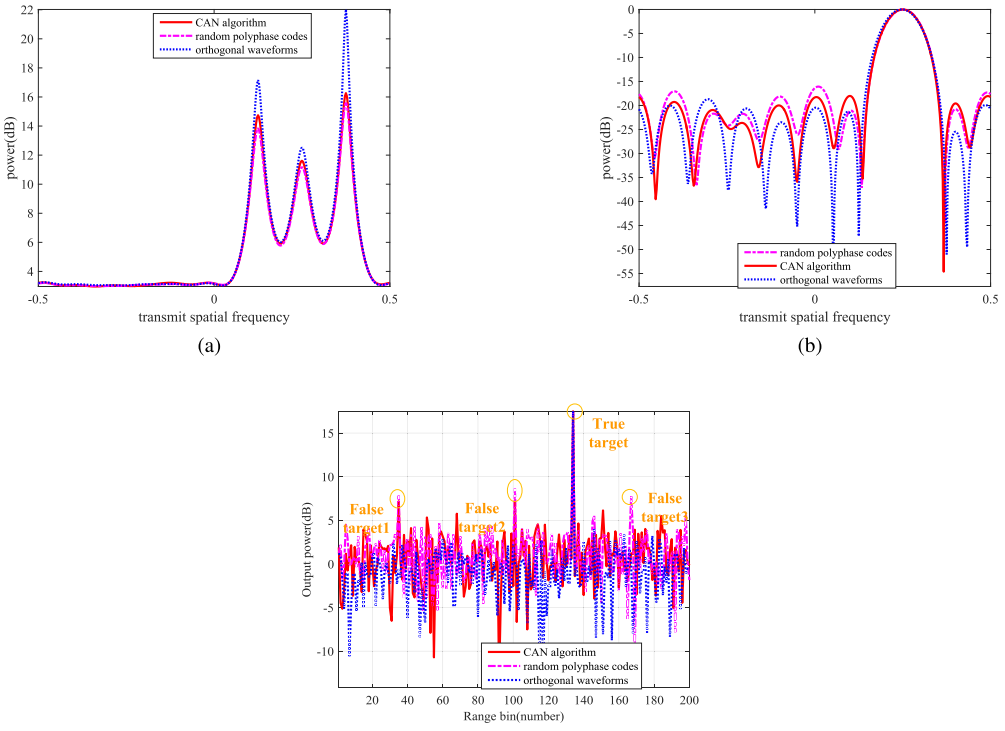

FIGURE 13. Comparison between perfectly orthogonal waveforms, random polyphase codes and CAN algorithm (a) Capon spectrum distributions; (b) Beam-patterns; (c) Output powers of range-angle adaptive matched filter.

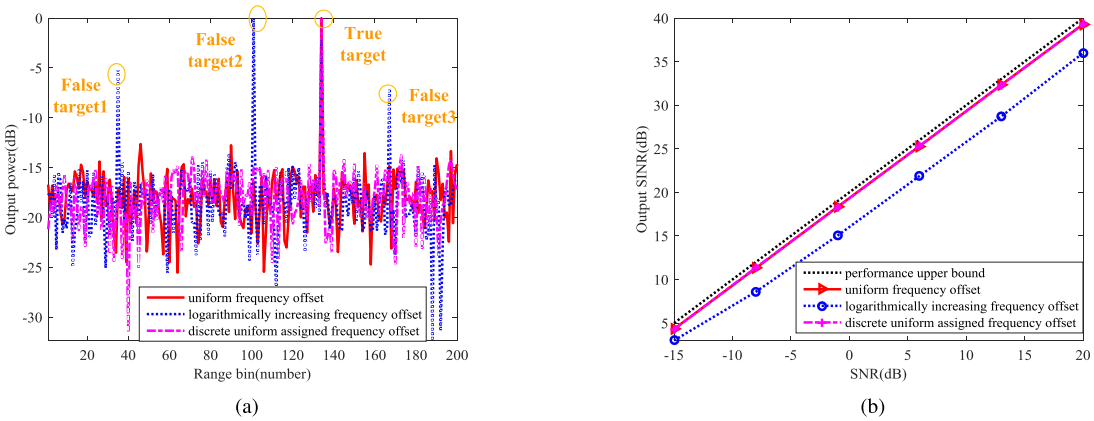

FIGURE 14. Results comparison for frequency offset optimization strategies. (a) Output power of range-angle adaptive matched filter; (b) Output SINR versus input SNR performance.

the range-angle 2-D beamforming, only the target with the specific range and angle can be detected and the deceptive jamming is suppressed due to mismatch in range. Furthermore, there is a null steering in $\theta_0 = 30°$, which means that the deceptive jamming both in the main-beam and side-lobes can be suppressed in the FDA-MIMO radar. As is shown in Fig. 9 (b), the covariance matrix contaminated by SOI makes the beam-former attempt to null the desired signal, leading to the beamforming distortion. Fig. 9 (d) compares the beam-patterns with the traditional processing, the adaptive NSD method and the robust NSD method. It can also be found that the beam-pattern with the robust NSD method has the lowest integrated side-lobe ratio.

The output power through the transmit-receive 2-D matched filter is presented in Fig.10, which indicates that the proposed approach is able to efficiently suppress the deceptive jamming. The comparison among Figs.10 (a), (b) and (c) shows that the true target can be easily detected in the range-angle domain by the robust NSD method. Meanwhile, the deceptive jamming can be suppressed due to mismatch in both range and angle. The output power for the detected target is influenced by the target cancellation without extraction

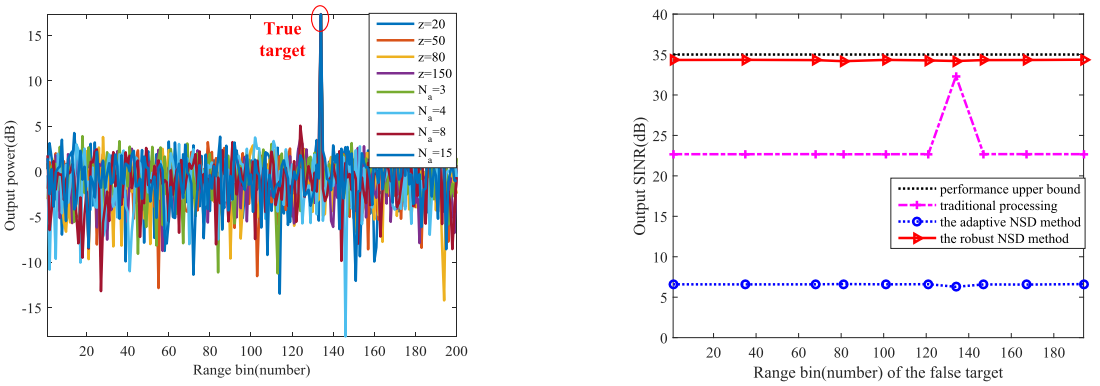

FIGURE 15. Results comparison in different scenarios. (a) Comparison of different frequency increments; (b) Comparison of different range bins of the false target.

of the SOI. Furthermore, shown in Fig.10 (d), if the robust nonhomogeneous samples selection strategy is not carried out, the detection performance degrades, which results in increased levels of the deceptive jamming.

Fig. 11 shows the output signal-to-interference-plus-noise ratio (SINR) of various approaches versus input signal-to-noise ratio (SNR) performance by Monte Carlo tests. The ideal case performance is provided for comparison. As to the traditional method without samples selection, the original samples from the whole range bins are used to estimate the covariance matrix. Thus, the performance degrades when the SNR of target is too high. It can also be seen that in the adaptive NSD method, the performance loss is considerable because of the self-cancellation phenomenon. In contrast, in the robust NSD method, as the target signal is not in the secondary sample data, the target self-cancellation is avoided. Therefore, a satisfactory output SINR performance is obtained, which is close to the upper bound. Moreover, its effective aperture is reduced because only a part of elements are utilized for matched filtering. However, since we perform smoothing once in transmit and receive domains, the performance loss is considerable due to the aperture loss.

B. SUPPRESSION PERFORMANCE ANALYSIS WITH THE FDA-MIMO RADAR

In this subsection, comparison results among different radar frameworks, including the conventional single-input single-output (SISO) radar, the conventional MIMO radar and the FDA-MIMO radar are given to show the advantages of the FDA-MIMO in the main-beam deceptive jamming suppression. Besides, comparison with perfectly orthogonal waveforms, random polyphase codes and the CAN algorithm are shown.

Fig. 12 compares the main-beam range deceptive jamming suppression results among the conventional SISO radar, the conventional MIMO radar and the FDA-MIMO radar. Shown in Figs. 12 (a) and (b), for the traditional collocated MIMO radar where the transmit spatial frequency is independent of range, it can be seen that the targets in the joint transmit-receive spatial frequency domain are diagonally distributed and the range ambiguity cannot be resolved [33]. Fig. 12 (c) and (d) show the beam-patterns and the output power of matched filter at $\theta_0 = 0°$, respectively. For the SISO radar, the output powers for the false targets from other angles are high due to the limited DOFs in the angle domain, which in turn generates high false-alarm ratios. For the conventional MIMO radar, the deceptive jamming in sidelobes, such as the false target 3, can be effectively suppressed. However, the main-beam deceptive jamming cannot be mitigated because it cannot provide any DOFs in range domain. In contrast, the FDA-MIMO radar is able to utilize the extra DOFs in the range and angle domains to suppress the main-beam deceptive jamming.

Fig. 12 (e) plots the output SINR versus input SNR by Monte Carlo tests. Since the SISO radar cannot handle the jamming, it yields to the lowest output SINR. Unlike the conventional SISO radar, the FDA-MIMO radar is capable of efficiently suppressing the false targets in the main-beam, eventually leading to high output SINR.

C. PERFORMANCE COMPARISON AMONG DIFFERENT INFLUENCE FACTORS

In this subsection, several influence factors are compared to investigate in detail the proposed method, i.e. the effect of different operational parameters is investigated. Fig. 13 demonstrates the comparison results of the suppression performance between the perfectly orthogonal waveforms, random polyphase codes and CAN algorithm at $\theta_0 = 0°$. Note that, it is assumed that the original samples are used. It can be seen from Fig. 13 (a) that the Capon spectrum degrades with non-perfectly orthogonal waveforms. Moreover, the sidelobes with non-perfectly orthogonal waveforms in Fig. 13 (b) are higher compared than those with the perfectly orthogonal waveforms. Shown in Fig 13 (c), for non-perfectly orthogonal waveforms, there is surplus of deceptive jamming without the selection of the

nonhomogeneous samples. Thus, proper MIMO waveforms should be designed to improve the performance.

In order to investigate the performance of the proposed approach thoroughly, comparison results with other existing methods in the FDA radar are provided. As for the frequency increments with the logarithmically increasing frequency offset (log-FDA) which was proposed in [20] and the discrete uniform distribution (discrete uniform-FDA) in [23], it can be seen from Fig. 14 (a) that the output power of the false targets are high with the log-FDA and the output SINR is low in Fig. 14 (b). Besides, Monte Carlo experiments with 200 trials are carried out in Fig. 15 to present the results in different scenarios. Shown in Fig. 15 (a), frequency increments vary with different z and N_a, which leads to different spatial frequency differences according to Eq. (20). Owing to the DOFs in the range domain introduced by the frequency increment in the FDA-MIMO radar, the main-beam deceptive jamming with different frequency increments can be effectively suppressed and the maximum power is obtained at the target. Furthermore, simulations are carried out to show the output SINR of various approaches versus different range bins of the false target. It is assumed that there is only one false target which can be located at different range bins. It can be seen from Fig. 15 (b) that the output SINR performance of the robust NSD method outperforms the other two methods. Note that, when the false target is located at the same range bin with the true target (No. 134), the target self-cancellation phenomenon arises, which leads to a sudden increase in the value of the output SINR in the adaptive NSD method.

V. CONCLUSIONS

In this paper, an innovative approach to suppress the main-beam deceptive jamming is proposed utilizing the range-angle-dependent characteristic of the FDA-MIMO radar and the nonhomogeneous sample detection. In particular, the case of non-perfectly orthogonal waveforms is considered. The proposed approach to main-beam deceptive jamming includes two steps, i.e., 1) distinguishing the true and false targets in the joint transmit-receive spatial frequency domain according to the time delay or range difference; 2) suppressing the false targets through an adaptive 2-D matched filtering. A robust NSD method is proposed to estimate the jamming-plus-noise covariance matrix. It is characterized by selecting all the nonhomogeneous samples and rejecting those including the signal. Results show that compared with traditional radar frameworks, the main-beam deceptive jamming can be effectively suppressed due to range mismatch in the FDA-MIMO radar. Furthermore, an output SINR improvement is obtained with the adaptive NSD method. Simulations characterizing various operational parameters have been run to demonstrate the advantages of the proposed method.

The deceptive jamming suppression is considered in the presence of Gaussian white noise in this paper. Future studies need to be carried out for more complex types of noise and clutter environment. Furthermore, the detection performances under different false alarm rates will be also considered. Specific approaches to design suitable waveforms for the purpose of jamming suppression will also be investigated.

REFERENCES

[1] L. Neng-Jing and Z. Yi-Ting, "A survey of radar ECM and ECCM," *IEEE Trans. Aerosp. Electron. Syst.*, vol. 31, no. 3, pp. 1110–1120, Jul. 1995.

[2] G. V. Morris and T. A. Kastle, "Trends in electronic counter-countermeasures," in *Proc. Nat. Telesyst. Conf. (NTC)*, Atlanta, GA, USA, Mar. 1991, pp. 265–269.

[3] J. Schuerger and D. Garmatyuk, "Deception jamming modeling in radar sensor networks," in *Proc. IEEE Military Commun. Conf.*, San Diego, CA, USA, Nov. 2008, pp. 1–7.

[4] K. Olivier, J. E. Cilliers, and D. M. Plessis, "Design and performance of wideband DRFM for radar test and evaluation," *Electron. Lett.*, vol. 47, no. 14, pp. 824–825, Jul. 2011.

[5] S. D. Berger and D. E. Meer, "An expression for the frequency spectrum of a digital radio frequency memory signal," in *Proc. IEEE Nat. Aerosp. Electron. Conf.*, Dayton, OH, USA, May 1990, pp. 90–93.

[6] M. Soumekh, "SAR-ECCM using phase-perturbed LFM chirp signals and DRFM repeat jammer penalization," *IEEE Trans. Aerosp. Electron. Syst.*, vol. 42, no. 1, pp. 191–205, Jan. 2006.

[7] K.-W. Lee, J.-H. Song, and W.-K. Lee, "Waveform diversity for SAR ECCM based on random phase and code rate transition," in *Proc. Eur. Radar Conf.*, London, U.K., 2016, pp. 286–289.

[8] Q. Feng, H. Xu, Z. Wu, B. Sun, "Deceptive jamming suppression for SAR based on time-varying initial phase," in *Proc. IEEE Int. Geosci. Remote Sens. Symp. (IGARSS)*, Beijing, China, Jul. 2016, pp. 4996–4999.

[9] A. Ahmed, Y. Zhao, R. Mohammed, and T. Bin, "An improved radar eccm method based on orthogonal pulse block and parallel matching filter," *J. Commun.*, vol. 10, no. 8, pp. 610–614, 2015.

[10] Z. Xiang, B. Chen, and M. Yang, "Transmitter/receiver polarisation optimisation based on oblique projection filtering for mainlobe interference suppression in polarimetric multiple-input-multiple-output radar," *IET Radar, Sonar Navigat.*, vol. 12, no. 1, pp. 137–144, 2018.

[11] J. Schuerger and D. Garmatyuk, "Performance of random OFDM radar signals in deception jamming scenarios," in *Proc. IEEE Radar Conf.*, Pasadena, CA, USA, May 2009, pp. 1–6.

[12] Y. Li, X. Jia, Y. Chen, and C. Yin, "Frequency agility MIMO-SAR imaging and anti-deception jamming performance," in *Proc. 31st URSI General Assembly Sci. Symp. (URSI GASS)*, Beijing, China, 2014, pp. 1–4.

[13] S. Zhao, L. Zhang, Y. Zhou, and N. Liu, "Measurement fusion method against false-target jamming for radar network," *J. Univ. Electron. Sci. Technol. China*, vol. 43, no. 2, pp. 865–869, Mar. 2014.

[14] B. Rao, S. Xiao, and X. Wang, "Joint tracking and discrimination of exoatmospheric active decoys using nine-dimensional parameter augmented EKF," *Signal Process.*, vol. 91, pp. 2247–2258, Oct. 2011.

[15] L. Bo, S. Yao, and Z. Chang-you, "Study of multistatic radar against velocity-deception jamming," in *Proc. Int. Conf. Electron., Commun. Control (ICECC)*, 2011, pp. 1044–1047.

[16] P. Antonik, M. C. Wicks, H. D. Griffiths, and C. J. Baker, "Frequency diverse array radars," in *Proc. IEEE Radar Conf.*, Verona, NY, USA, Apr. 2006, pp. 215–217.

[17] T. Higgins and S. D. Blunt, "Analysis of range-angle coupled beamforming with frequency diverse chirps," in *Proc. 4th Int. Waveform Diversity Des. Conf.*, Feb. 2009, pp. 140–144.

[18] M. C. Wicks and P. Antonik, "Frequency diverse array with independent modulation of frequency, amplitude, and phase," U.S. Patent 7 319 427, Jan. 15, 2008.

[19] B. Chen, X. Chen, Y. Huang, and J. Guan, "Transmit beampattern synthesis for the FDA radar," *IEEE Antennas Wireless Propag. Lett.*, vol. 17, no. 1, pp. 98–101, Jan. 2018.

[20] W. Khan, I. M. Qureshi, and S. Saeed, "Frequency diverse array radar with logarithmically increasing frequency increment," *IEEE Antennas Wireless Propag. Lett.*, vol. 14, pp. 499–502, 2015.

[21] A. Yao, W. Wu, and D. Fang, "Frequency diverse array antenna using time-modulated optimized frequency offset to obtain time-invariant spatial fine focusing beampattern," *IEEE Trans. Antenna Propag.*, vol. 64, no. 10, pp. 4434–4446, Oct. 2016.

[22] H. Shao, J. Dai, J. Xiong, H. Chen, and W.-Q. Wang, "Dot-shaped range-angle beampattern synthesis for frequency diverse array," *IEEE Antennas Wireless Propag. Lett.*, vol. 15, pp. 1703–1706, Feb. 2016.
[23] Y. Liu, H. Ruan, L. Wang, and A. Nehorai, "The random frequency diverse array: A new antenna structure for uncoupled direction-range indication in active sensing," *IEEE J. Sel. Topics Signal Process.*, vol. 11, no. 2, pp. 295–308, Mar. 2017.
[24] K. Gao, W.-Q. Wang, J. Cai, and J. Xiong, "Decoupled frequency diverse array range–angle-dependent beampattern synthesis using non-linearly increasing frequency offsets," *IET Microw., Antennas Propag.*, vol. 10, no. 8, pp. 880–884, Jun. 2016.
[25] J. J. Huang, K. F. Tong, and C. J. Baker, "Frequency diverse array: Simulation and design," in *Proc. Int. Antennas Propag. Radar conf. (RADAR)*, Pasadena, CA, USA, 2009, pp. 1–4.
[26] C. Y. Mai, S. T. Lu, J. P. Sun, and G. H. Wang, "Beampattern optimization for frequency diverse array with sparse frequency waveforms," *IEEE Access*, vol. 5, p. 17914–17926, 2017.
[27] A. M. Jones and B. D. Rigling, "Frequency diverse array radar receiver architectures," in *Proc. WDD Conf.*, Jan. 2012, pp. 211–217.
[28] J. Xiong, W.-Q. Wang, and K. Gao, "FDA-MIMO radar range—Angle estimation: CRLB, MSE, and resolution analysis," *IEEE Trans. Aerosp. Electron. Syst.*, vol. 54, no. 1, pp. 284–294, Feb. 2018.
[29] W. Q. Wang, "Subarray-based frequency diverse array radar for target range-angle estimation," *IEEE Trans. Aerosp. Electron. Syst.*, vol. 50, no. 4, pp. 3057–3067, Oct. 2014.
[30] A. Basit, I. M. Qureshi, W. Khan, and A. N. Malik, "Range-angle-dependent beamforming for cognitive antenna array radar with frequency diversity," *Int. J. Antennas Propag.*, vol. 8, no. 2, pp. 204–216, Aug. 2016.
[31] J. Farooq, M. A. Temple, and M. A. Saville, "Exploiting frequency diverse array processing to improve SAR image resolution," in *Proc. IEEE Radar Conf.*, May 2008, pp. 1–5.
[32] J. Xu, S. Zhu, and G. Liao, "Range ambiguous clutter suppression for airborne FDA-STAP radar," *IEEE J. Sel. Topics Signal Process.*, vol. 9, no. 8, pp. 1620–1631, Dec. 2015.
[33] J. Xu, G. Liao, S. Zhu, L. Huang, and H. C. So, "Joint range and angle estimation using MIMO radar with frequency diverse array," *IEEE Trans. Signal Process.*, vol. 63, no. 13, pp. 3396–3410, Jul. 2015.
[34] J. Xu, S. Zhu, and G. Liao, "Space-time-range adaptive processing for airborne radar systems," *IEEE Sensors J.*, vol. 15, no. 3, pp. 1602–1610, Mar. 2015.
[35] A. Abdalla, W.-Q. Wang, Z. Yuan, S. Mohamed, and T. Bin, "Subarray-based FDA radar to counteract deceptive ECM signals," *EURASIP J. Adv. Signal Process.*, p. 104, Dec. 2016. [Online]. Available: https://doi.org/10.1186/s13634-016-0403-6
[36] S. Li, L. Zhang, N. Liu, J. Zhang, and S. Zhao, "Adaptive detection with conic rejection to suppress deceptive jamming for frequency diverse MIMO radar," *Digit. Signal Process.*, vol. 69, pp. 32–40, Oct. 2017.
[37] M. Akćakaya and A. Nehorai, "MIMO radar sensitivity analysis for target detection," *IEEE Trans. Signal Process.*, vol. 59, no. 7, pp. 3241–3250, Jul. 2011.
[38] K. Gerlach, "Outlier resistant adaptive matched filtering," *IEEE Trans. Aerosp. Electron. Syst.*, vol. 38, no. 3, pp. 885–901, Jul. 2002.
[39] D. J. Rabideau and A. O. Steinhardt, "Improving the performance of adaptive arrays in nonstationary environments through data-adaptive training," in *Proc. 13th Asilomar Conf. Signals, Syst. Comput.*, Pacific Grove, CA, USA, Nov. 1996, pp. 75–79.
[40] P. Chen and M. C. Wicks, "A procedure for detecting the number of signal components in a radar measurement," in *Proc. IEEE Int. Radar Conf.*, Alexandra, VA, USA, May 2000, pp. 451–456.
[41] M. C. Wicks, W. L. Melvin, and P. Chen, "An effective architecture for nonhomogeneity detection in space-time adaptive processing airborne early warning radar," in *Proc. Int. Radar Conf.*, Edinburgh, U.K., 1997, pp. 295–299.
[42] M. Rangaswamy, B. Himad, and J. H. Michels, "Performance analysis of the nonhomogeneity detector for STAP applications," in *Proc. Nat. Radar Conf.*, 2001, pp. 193–197.
[43] W. L. Melvin and M. C. Wicks, "Improving practical space-time adaptive radar," in *Proc. IEEE Nat. Radar Conf.*, Syracuse, NY, USA, May 1997, pp. 48–53.
[44] T. K. Sarkar *et al.*, "A deterministic least-squares approach to space-time adaptive processing (STAP)," *IEEE Trans. Antennas Propag.*, vol. 49, no. 1, pp. 91–103, Jan. 2001.
[45] K. Gerlach, "The effects of signal contamination on two adaptive detectors," *IEEE Trans. Aerosp. Electron. Syst.*, vol. 30, no. 1, pp. 297–309, Jan. 1995.
[46] S. A. Vorobyov, "Principles of minimum variance robust adaptive beamforming design," *Signal Process.*, vol. 93, no. 12, pp. 3264–3277, 2013.
[47] D. Cristallini and W. Burger, "A robust direct data domain approach for STAP," *IEEE Trans. Signal Process.*, vol. 60, no. 3, pp. 1283–1294, Mar. 2012.
[48] H. He, P. Stoica, and J. Li, "Designing unimodular sequence sets with good correlations—Including an application to MIMO radar," *IEEE Trans. Signal Process.*, vol. 57, no. 11, pp. 4391–4405, Nov. 2009.
[49] J. Xu, G. Liao, Y. Zhang, H. Ji, and L. Huang, "An adaptive range-angle-Doppler processing approach for FDA-MIMO radar using three-dimensional localization," *IEEE J. Sel. Topics Signal Process.*, vol. 11, no. 2, pp. 309–320, Mar. 2017.
[50] L. L. Scharf, *Statistical Signal Processing: Detection, Estimation and Time Series Analysis*. Reading, MA, USA: Addison Wesley, 1991.

LAN LAN was born in Xi'an, China, in 1993. She received the B.S. degree in electronic engineering from Xidian University, Xi'an, in 2015, where she is currently pursuing the Ph.D. degree with the National Laboratory of Radar Signal Processing. Her research interests include frequency diverse array radar systems, MIMO radar signal processing, and ECCM.

GUISHENG LIAO (M'96–SM'16) was born in Guilin, Guangxi, China, in 1963. He received the B.S. degree from Guangxi University, Guangxi, in 1985, and the M.S. and Ph.D. degrees from Xidian University, Xi'an, China, in 1990 and 1992, respectively. He has been a Senior Visiting Scholar with the Chinese University of Hong Kong, Hong Kong. He is currently a Professor with the National Laboratory of Radar Signal Processing, Xidian University. His research interests include array signal processing, space-time adaptive processing, SAR ground moving target indication, and distributed small satellite SAR system design. He is a member of the National Outstanding Person and the Cheung Kong Scholars in China.

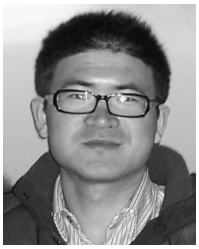

JINGWEI XU (M'15) was born in Shangdong, China, in 1987. He received the B.S. degree in electronic and information engineering and the Ph.D. degree in signal and information processing from Xidian University, China, in 2010 and 2015, respectively. He is currently a Post-Doctoral Researcher with the National Laboratory of Radar Signal Processing, Xidian University. His research interests include robust adaptive beamforming, frequency diverse array radar systems, STAP-based radar signal processing, and MIMO radar signal processing.

YUHONG ZHANG (SM'96) received the B.S., M.S., and Ph.D. degrees in electrical engineering from Xidian University, Xi'an, China, in 1982, 1984, and 1988, respectively. From 1998 to 2014, he was a Senior Scientist at Stiefvater Consultants, and a Research Associate with Defense Conversion Inc., Rome, NY, USA, and involved in on-site at the Air Force Research Laboratory, Rome, from 1998 to 2010. From 1994 to 1998, he was at Syracuse University, Syracuse, NY, USA, as a Visiting Associate Professor. From 1988 to 1993, he was with the Institute of Electronic Engineering, Xidian University, and served as an Associate Professor and the Deputy Director of the Institute. He is currently a Professor with the School of Electronic Engineering, Xidian University. His current research interests include array signal processing, remote sensing, signal modeling and simulation, SAR imaging, and waveform diversity.

FRANCESCO FIORANELLI (M'17) received the bachelor's and master's degrees *(summa cum laude)* in telecommunication engineering from the Università Politecnica delle Marche, Ancona, Italy, in 2007 and 2010, respectively, and the Ph.D. degree in throughwall radar imaging from Durham University, U.K., in 2014. He was a Research Associate on multistatic radar with Prof. H. Griffiths at University College London, from 2014 to 2016. He then joined the University of Glasgow in 2016 as a Lecturer/Assistant Professor with the Glasgow College UESTC, between the University of Glasgow and the University of Electronic Science and Technology of China (UESTC), Chengdu. He has authored or co-authored over 35 journal and conference papers in various applications and aspects of radar systems, as well as two book chapters. His research interests include human micro-Doppler signatures and classification for security and healthcare applications, UAVs detection and classification, through-wall radar, wind farm clutter, and sea clutter characterization and mitigation. He is a member of IET, a Chartered Engineer, an Associate Member of the EPSRC Peer Review College since 2017, and a Reviewer for several academic journals, including *IET Radar, Sonar & Navigation*, the IEEE TRANSACTIONS ON AEROSPACE AND ELECTRONIC SYSTEMS, and the IEEE SENSORS.